J Mater Sci: Mater Med (2009) 20:691–697
DOI 10.1007/s10856-008-3619-7

Electrophoretic deposition of silicon-substituted hydroxyapatite/poly(ε-caprolactone) composite coatings

Xiufeng Xiao · Rongfang Liu · Xiaolian Tang

Received: 6 July 2008 / Accepted: 6 October 2008 / Published online: 24 October 2008

Abstract Silicon-substituted hydroxyapatite/poly(ε-caprolactone) composite coatings were prepared on titanium substrate by electrophoretic deposition in *n*-butanol and chloroform mixture. The effect of the concentration of poly(ε-caprolactone) in suspension on the morphology and the microstructure of coatings were investigated, furthermore, the thermal behavior and in vitro bioactivity were also investigated. The results show that the coarse and accidented silicon-substituted hydroxyapatite/poly(ε-caprolactone) composite coatings were obtained by electrophoretic deposition when the concentration of poly(ε-caprolactone) in suspension was 6–16 g/l. The adsorption of poly(ε-caprolactone) on the surface of Si–HA particles hinders the electrophoretic deposition of Si–HA. The shear-testing experiments indicated that the addition of poly(ε-caprolactone) in suspension is in favor of improving the bonding strength of the coatings. After immersion in simulated body fluid for 8 days, silicon-substituted hydroxyapatite/poly (ε-caprolactone) composite coatings have the ability to induce the bone-like apatite formation.

1 Introduction

Hydroxyapatite ($Ca_{10}(PO_4)_6(OH)_2$, HA) is a major inorganic component of natural bone, HA is recognized as osteoconductive and able to accelerate bone in growth and attachment to the surface of implant during the early stages after implantation[1, 2]. However, its mechanical strength is too poor to use in load-bearing prostheses, therefore, significant research activity has been associated with the development of HA coatings. In the past three decades, many coating procedures have been documented, but all have shortcomings [3].

Electrophoretic deposition (EPD) is known to be one of the most effective and efficient techniques to assemble fine particles. This technique has received significant attention due to its simplicity in setup, low equipment cost, and capability to form complex shapes and patterns [4–6]. Wei et al. [7] used HA nanoparticles to deposit HA dual-coating on metal substrates by EPD, and studied the interfacial bond strength of the coatings. Hamagami et al. [8] fabricated highly ordered macroporous apatite coating onto titanium by EPD. However, EPD cannot be used for the fabrication of dense coatings on metals due to the sintering shrinkage, chemical reactions between the coatings and the substrates, and other problems discussed in the literature [9–11]. These problems can be eliminated by the fabrication of polymer–ceramic composites [12]. The use of polymers offers the advantage of low temperature processing of composite materials. By coating with plastic polymer layer, the brittleness of the apatite is expected to be overcome.

In recent years, there is a tendency to develop ceramic-polymer composite coatings on titanium substrate in order to obtain new type of coatings [13]. Ceramic–polymer composite coatings impart other functional properties to the implants, such as chemical stability, bioactivity, biocompatibility, and antimicrobial properties [14]. Sewing et al. [15, 16] reported a multi-layer collagen/calcium phosphate coating on titanium where the collagen was physically absorbed on the surface followed by electrolytic deposition of a calcium phosphate layer. Lin et al. [17] prepared hybrid bioceramic coating of hydroxyapatite

X. Xiao · R. Liu (✉) · X. Tang
College of Chemistry and Materials Science,
Fujian Normal University, Fuzhou 350007, China
e-mail: rfliu@vip.sina.com

(HA)/poly(vinylacetate) on the surface of Ti–6Al–4V alloy in order to improve the adhesion between the HA coating and the metal substrate. The shear-testing experiments indicated that the bonding strength of the hybrid coating to metal substrate was increased by as much as 3 MPa. Yousefpour et al. [3] reported that a synergistic effect of co-deposition of HA coating and vinyl acetate polymer might exhibit improved crystallization of HA coating, with better bioactivity. Several investigations were focused on the fabrication of HA–chitosan coatings [18, 19]. Electrochemical precipitation methods were developed for the formation of calcium phosphate–chitosan composites, which can be converted to HA–chitosan coatings by heating in aqueous solutions of sodium hydroxide [18]. Another approach is based on EPD of HA nanoparticles and chitosan macromolecules [20]. Zhitomirsky et al. [14] reported the HA–chitosan coatings using a combined method, based on the EPD of HA and electrochemical deposition of chitosan. The co-deposition of HA and chitosan enabled the room-temperature fabrication of advanced coatings by EPD [14, 20]. Therefore, the problems related to the high-temperature sintering can be avoided.

In a previous investigation [21], we have discovered a possibility to fabricate silicon-substituted hydroxyapatite (Si–HA) coatings by EPD in a high stable suspension containing fine Si–HA particles using *n*-butanol and chloroform as medium and triethanolamine (TEA) as the additive. Owing to the chloroform solvent properties, some biodegradable polymer, such as polylactic acid (PLA), polycaprolactone (PCL) could be dissolved in the medium, so that the HA and the polymer could be co-deposited on a titanium substrate by EPD. The objective of this study is to develop a method for the preparation of HA–polymer composite coatings on the titanium implants. The morphological change, microstructure, and bioactivity of the composite coatings were investigated. Si–HA was employed because the studies carried out by Carlisle [22] indicated the importance of the silicon on bone formation and calcification. The use of Si–HA as a biomaterial has been reported recently [23–26]. However, the study of depositing Si–HA coatings onto metallic surface have been few reported [21, 27]. The PCL was attractive due to its low cost, sustained biodegradability, and availability at low molecular weight [28, 29].

2 Materials and methods

2.1 Preparation of 0.8 wt% Si–HA nanoparticles

The procedure for preparation of 0.8 wt% Si–HA nanoparticles were based on that previously described [30]. The Si–HA nanoparticles were prepared by hydrothermal reaction of $Ca(NO_3)_2 \cdot 4H_2O$, $(NH_4)_3PO_4$ and $Si(OCH_2CH_3)_4$ (TEOS) solutions. The quantities of reactants were calculated by assuming that silicon (or silicate) would substitute for phosphorus (or phosphate). The $Ca(NO_3)_2 \cdot 4H_2O$ solution was added to $(NH_4)_3PO_4$ and TEOS mixed solutions while stirring at room temperature in a reactor. The mixtures were stirred for 0.5 h, then hydrothermal treatment at 200°C for 8 h. The resulting precipitates were filtered, dried at 100°C overnight.

2.2 Preparation of the coatings

1 g Si–HA powders were ultrasonic agitated in 34 ml *n*-butanol containing 15 ml l^{-1} triethanolamine and 0–0.8 g PCL was dissolved in 16 ml chloroform, and then these two solutions were mixed. The final concentration of PCL is 0–16 g/l. Deposits were made on 1 cm × 1 cm titanium substrates, which were abraded on SiC grit paper and then ultrasonicated in acetone and ethanol, washed with distilled water and then activated in 1:1(vol) H_2O_2/NH_3 solution at room temperature overnight, and dried in air at room temperature. The Si–HA powders were positively charged in the *n*-butanol and chloroform mixed medium, moving towards the cathode under the influence of the electric field and depositing there. Therefore, titanium substrate served as the cathode in a two electrode electrochemical cell. A 4 cm × 3 cm platinum plate was used as the parallel anode. The distance between the electrodes was 7.5 mm. Deposition was carried out for 90 s. For all deposition times the voltage was maintained at 30 V. After deposition, the coatings were washed with distilled water and dried in air at 50°C.

2.3 In vitro bioactivity tests

The in vitro bioactivity of Si–HA/PCL composite coatings were studied by immersing them into the simulated body fluid (SBF) for 8 days at 37°C without stirring before they were taken out for coating characteristics. The compositions of SBF are reported in literature [31]. The SBF solution was buffered at pH 7.4 with tri[hydroxymethyl]aminomethane $[(CH_2OH_3)_3CNH_3]$ and hydrochloric acid.

2.4 Sample characterization

The morphology of the coatings were characterized by Philips XL30 environmental scanning electron microscope (SEM). The microstructure and chemical composition were characterized by Philips X'Pert MPD X-ray diffractometer (XRD) and Nicolet Avatar 360 Fourier transform infrared spectroscope (FTIR). The thermal stability of the coatings

were measured by Mettler-Toledo 851e thermogravimetric and differential thermal analyzer (TG/DTA) at a heating rate of 10°C/min to 1,000°C in an N_2 atmosphere. The interfacial shear strength of the coatings were carried out with a materials testing machine (LR5KN) using a 10 kN load cell and a crosshead speed of 1.0 mm/min. For each testing material, three specimens were used, and the shear strength data was reported as the average value.

3 Results and discussion

3.1 SEM analysis

Figure 1 shows the SEM micrographs of the coatings prepared in the different content of PCL in suspensions, it can be seen that the surface of Si–HA coating without PCL is relatively smooth (Fig. 1a). The surface of Si–HA/PCL composite coatings are coarse and accidented and there are many pores in it (Fig. 1b, c). Si–HA particles are positively charged in suspensions which can move to cathode under an applied electric field. However, PCL is dissolved but not charged in *n*-butanol–chloroform mixture. It is suggested that only physical adsorption resulted in an accumulation of PCL at the cathode, and the Si–HA particles are wrapped in the PCL layer. The insulative property of PCL will prevent the electrophoretic deposition of Si–HA particles, and lead to the inhomogeneity of deposition, and the porosity of the composite coatings. When the content of PCL in suspension up to 16 g/l, the PCL layer increases with the content of PCL in suspension (Fig. 1d), but the surface of coatings have obvious crack (Fig. 1e). It is suggested that the increase in the PCL concentration in the solutions containing Si–HA particles can result in an increasing suspension viscosity, decreasing electrophoretic mobility, and thus decreasing deposition yield of Si–HA. Due to the difference of thermal behavior between PCL and Si–HA particles, the cracks in the composite coatings can be attributed to the drying shrinkage. Figure 1f shows the SEM micrograph of the cross-section of the composite coatings. It can be seen that the composite coating has this structure with relatively dense inner and loose outer. It also explains that the PCL adsorption on the surface of Si–HA particles hinder the electrophoretic deposition of Si–HA.

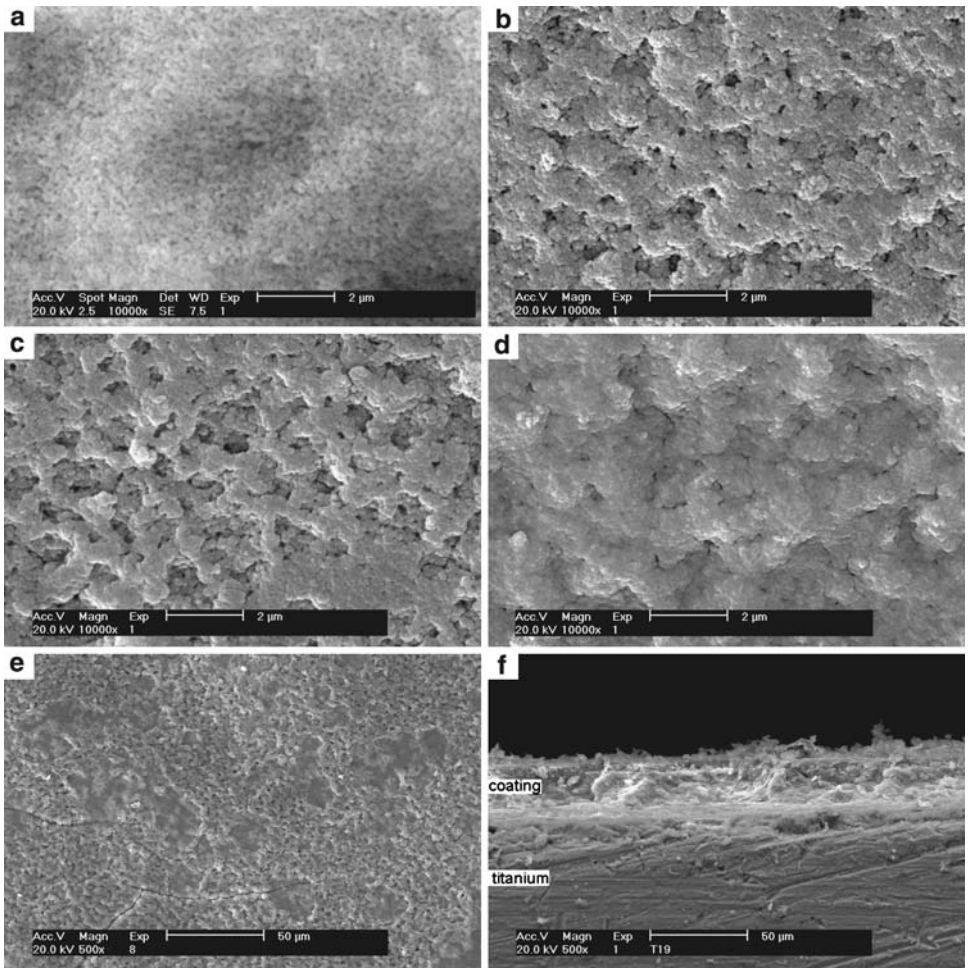

Fig. 1 SEM morphologies of Si–HA coating (**a**) and Si–HA/PCL composite coatings with different PCL content: **b** 6 g/l; **c** 12 g/l; **d**, **e** 16 g/l; **f** 12 g/l, cross section

3.2 XRD and FTIR analyses

Figure 2 shows the XRD patterns of the Si–HA coating and Si–HA/PCL composite coatings prepared in the different content of PCL in suspensions. For all samples, typical PCL and HA peaks appear. There were no other peaks or peak shifts in the composites, suggesting that no chemical reactions occur.

The FTIR spectra of the powders removed from the coatings are shown in Fig. 3. The adsorption peaks of hydroxyl, PO_4^{3-} and CO_3^{2-} groups can be obviously observed in all the spectra (Fig. 3a–c). The hydroxyl stretching and bending bands are observed at 3,571 and 631 cm^{-1}, respectively. The broad bands attributed to absorbed water are also found at 3,430 and 1,640 cm^{-1}. The bands of carbonate were observed at 1,450 cm^{-1} and 1,418 cm^{-1}, this is due to the substitution of phosphate groups (PO_4^{3-}) by carbonate (CO_3^{2-}). The TEOS reactant provides the CO_3^{2-} to the samples by hydrolysis [30]. The adsorption bands at 1091, 1034, 572, 470 cm^{-1} are ascribed to PO_4^{3-} groups. The band at 1,727 cm^{-1} (Fig. 3b, c) of Si–HA/PCL composite coatings can be attributed to C=O vibration modes of PCL. The hydroxyl stretching and bending bands intensities decrease with PCL concentration increasing from 6 g/l (Fig. 3b) to 12 g/l (Fig. 3c) in suspension. As shown in the XRD patterns, no band shifts are observed in the FTIR spectra, confirming that no chemical reactions occurred between Si–HA and PCL.

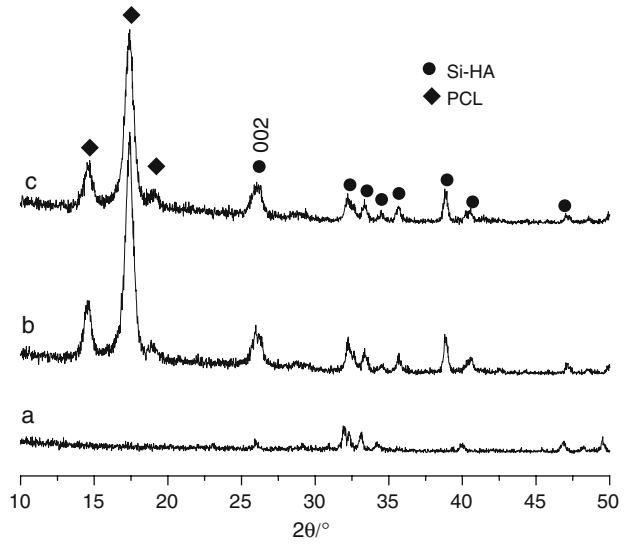

Fig. 2 XRD patterns of the Si–HA coating (a) and Si–HA/PCL composite coatings with different PCL content: (b) 6 g/l, (c) 12 g/l

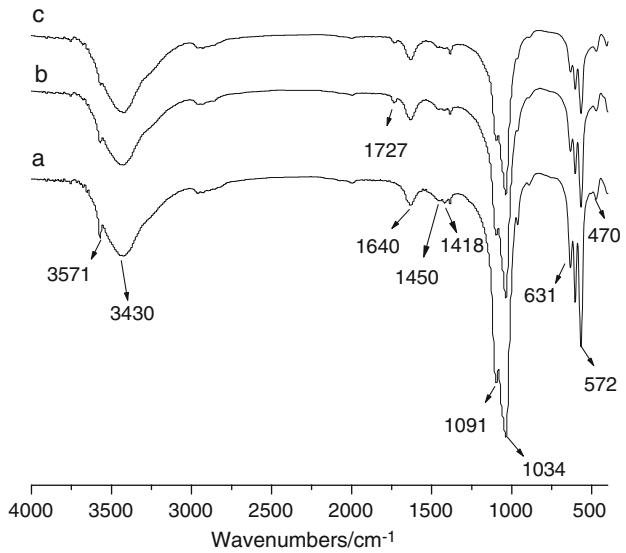

Fig. 3 FTIR spectra of Si–HA coating (a) and Si–HA/PCL composite coatings with different PCL content: (b) 6 g/l, (c) 12 g/l

3.3 TG/DTA analysis

Figure 4 compares the TG/DTA data for the Si–HA coating and the Si–HA/PCL composite coating electrophoretic deposited in 6 g/l PCL suspension. The total weight loss for the Si–HA coating at 500°C is about 1.75 wt%, which

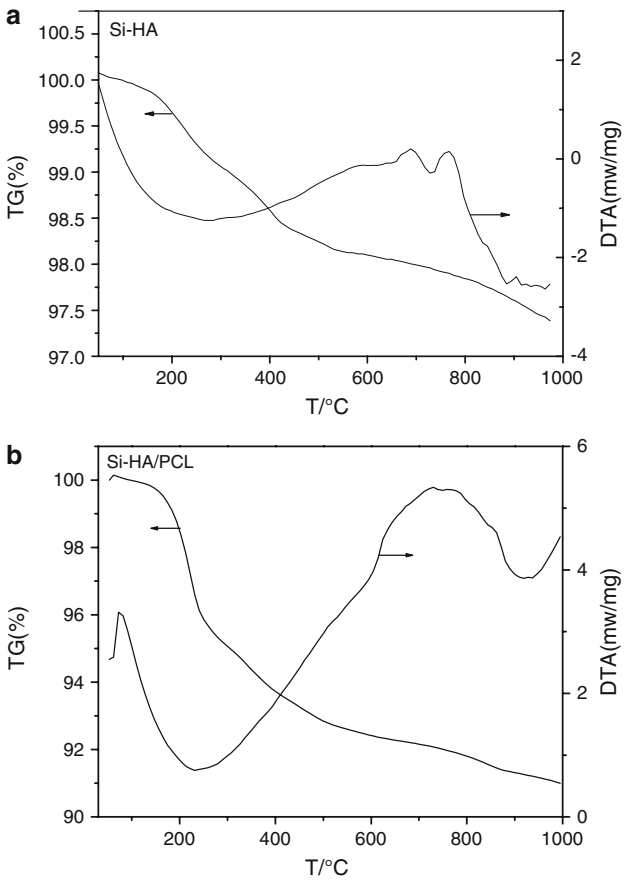

Fig. 4 DTA/TG curves of the Si–HA coating (**a**) and Si–HA/PCL composite coating deposited in 6 g/l PCL suspension (**b**)

can be attributed to the liberation of adsorbed water. The gradual decrease in weight from 500 to 900°C is a result of the slow elimination of the carbonate group linked to Si–HA, the presence of which has been confirmed by the FTIR analysis. A endothermic peak during 700–800°C in DTA curve (Fig. 4a) may correspond to the elimination of the carbonate group. The clear peaks that correspond to carbonate in the FTIR spectra of Si–HA powders disappear after heat treated at 800°C [30]. For the composite coatings, the TG curves show the total weight loss of 7.0 wt% at 500°C, indicating an additional step in weight loss. The additional weight loss for the composite coating compared to the Si–HA coating can be attributed to the burning out of PCL. The results of the TG investigations indicate the co-deposition of Si–HA and PCL. The PCL content in the composite coatings prepared in the 6 g/l PCL suspensions containing approximately 5.25 wt% PCL. The TG results are consistent with the DTA data. The DTA data for the composite coatings shows a broad endothermic peak during the range of 50–500°C, related to the burning out of PCL.

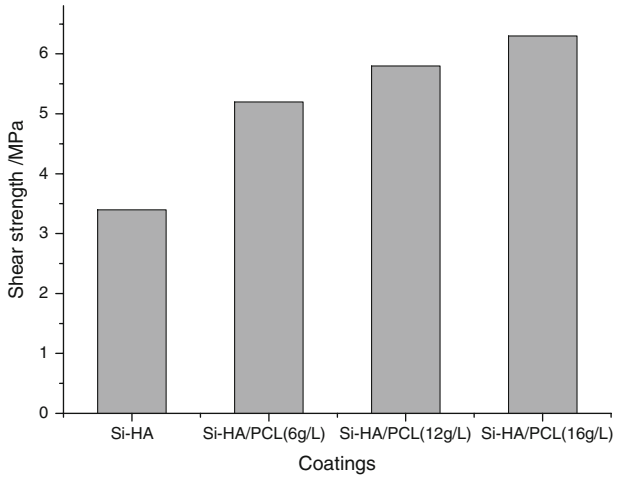

Fig. 5 The bonding strength of the Si–HA coating and Si–HA/PCL composite coatings

3.4 Bonding strength of the coatings

The bonding strength of the coatings and substrates, as measured by shear strength test, are shown in Fig. 5. If no addition of PCL are added in suspension, adhesion between the Si–HA coating and titanium substrate is poor. On average, the shear strength between Si–HA coating and substrate is only 3.4 Mpa. The evidence of shear strength improvement is by the addition of PCL in suspension. It is found that the bonding strength of the Si–HA/PCL composite coatings increase with increasing the concentration of PCL in suspension on the range of 6–16 g/l, which may be attributed to coarse and accidented surface of the Si–HA/PCL composite coatings (Fig. 1b–d). Furthermore, the ductile polymer is in favor of improving the cohesive force among the Si–HA particles.

3.5 Bioactivity of the composite coatings

After 8 days in vitro bioactive tests (immersion in SBF solutions), the SEM image shows that a dense deposits

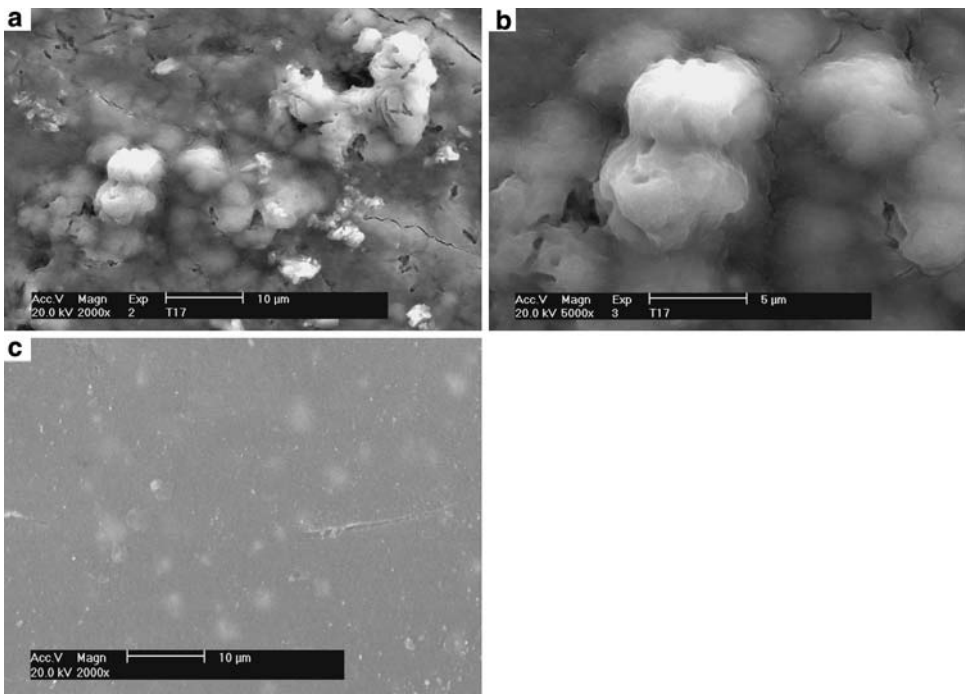

Fig. 6 SEM micrograph of Si–HA/PCL composite coating deposited in 12 g/l PCL suspension (**a**, **b**) and PCL film (**c**) after immersion in SBF for 8 days

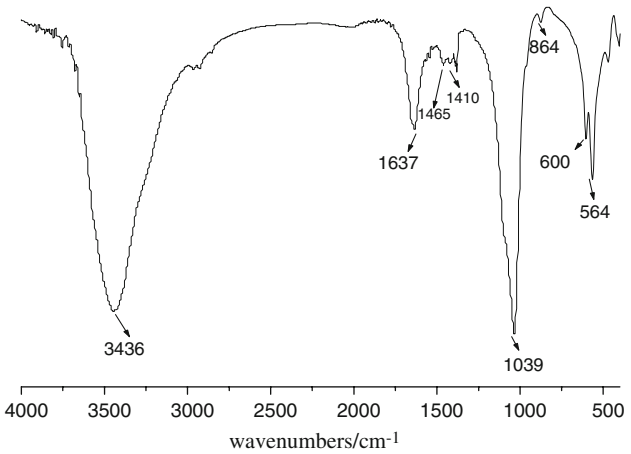

Fig. 7 FTIR spectrum of the scraped deposits after the Si–HA/PCL composite coating immersed in SBF for 8 days (the concentration of PCL in suspension: 12 g/l)

cover the composite coatings (Fig. 6a), such deposits are not observed prior to soaking in SBF (Fig. 1c). With high magnification, we can see that many spherical particles are accumulated on the surface of the coatings (Fig. 6b). The morphology is very similar to that of the deposited apatite on a substrate through biomimetic processing utilizing SBF [32]. The FTIR spectrum of the scraped deposits is shown in Fig. 7. The deposits show the absorption peak of PO_4^{3-} group at 564 cm^{-1}, 600 cm^{-1} and 1,039 cm^{-1}, CO_3^{2-} group at 864 cm^{-1}, 1,410 cm^{-1} and 1,465 cm^{-1}. The results indicate that the apatite formed on the composite coating is carbonated apatite. As a control experiment, the in vitro bioactive test of pure PCL film covered on the titanium substrate is carried out. There are not any deposits formed on the surface of PCL film (Fig. 6c). The induction required for the apatite nucleation is dependent on the functional groups. PCL is a bioinert material, without the functional groups required for inducing apatite formation. Therefore, the formation of the bone-like apatite at the surface of the composite coating is induced by the presence of Si–HA particles.

4 Conclusion

Si–HA/PCL composite coatings were obtained by electrophoretic deposition in *n*-butanol and chloroform mixture. The PCL adsorption on the surface of Si–HA particles hinders the electrophoretic deposition of Si–HA. TG/DTA results show that the PCL content in the composite coatings prepared in the 6 g/l PCL suspensions contains approximately 5.25 wt% PCL. XRD and FTIR results show that there were no chemical reactions occurred between Si–HA nanoparticles and PCL. The Si–HA/PCL composite coatings exhibit a better bonding strength than Si–HA coating. In vitro bioactivity tests show that Si–HA/PCL composite coatings have good bioactivity.

Acknowledgements We thank National Nature Science Foundation of China (30600149), the Science Research Foundation of Ministry of Health & United Fujian Provincial Health and Education Project for Tackling the Key Research, P.R. China (WKJ 2005-2-008), Fujian Development and Reform Commission of China (No. 2004[477]) and Fujian Provincial Department of Science and Technology (No. 2006I0015).

References

1. K.J.L. Burg, S. Porter, J.F. Kellam, Biomaterials **21**, 2347 (2000). doi:10.1016/S0142-9612(00)00102-2
2. Y. Liu, D. Hou, G. Wang, Mater. Chem. Phys. **86**, 69 (2004). doi:10.1016/j.matchemphys.2004.02.009
3. A. Afshar, M. Yousefpour, X.D. Yang, X.D. Li, B.C. Yang, Y. Wu, J.Y. Chen, X.D. Zhang, Mater. Sci. Eng. B **128**, 243 (2006). doi:10.1016/j.mseb.2005.11.022
4. C. Kaya, F. Kaya, B. Su, B. Thomas, A.R. Boccaccini, Surf. Coat Technol. **191**, 303 (2005). doi:10.1016/j.surfcoat.2004.03.042
5. G. Cao, J. Phys. Chem. B **108**, 19921 (2004). doi:10.1021/jp040492s
6. I. Singh, C. Kaya, M.S.P. Shaffer, B.C. Thomas, A.R. Boccaccini, J. Mater. Sci. **41**, 8144 (2006). doi:10.1007/s10853-006-0170-0
7. M. Wei, A.J. Ruys, M.V. Swain, S.H. Kim, B.K. Milthorpe, C.C. Sorrell, J. Mater. Sci.: Mater. Med. **10**, 401 (1999). doi:10.1023/A:1008923029945
8. J. Hamagami, Y. Ato, K. Kanamura, Solid State Ion. **172**, 331 (2004). doi:10.1016/j.ssi.2004.02.046
9. P. Ducheyne, S. Radin, M. Heughebaert, J.C. Heughebaert, Biomaterials **11**, 244 (1990). doi:10.1016/0142-9612(90)90005-B
10. I. Zhitomirsky, L. Gal-Or, J. Mater. Sci.: Mater. Med. **8**, 213 (1997). doi:10.1023/A:1018587623231
11. C.S. Kim, P. Ducheyne, Biomaterials **12**, 461 (1991). doi:10.1016/0142-9612(91)90143-X
12. X. Pang, I. Zhitomirsky, Mater. Chem. Phys. **94**, 245 (2005). doi:10.1016/j.matchemphys.2005.04.040
13. X. Lu, Y.B. Wang, Y.R. Liu, J.X. Wang, S.X. Qu, B. Feng, J. Weng, Mater. Lett. **61**, 3970 (2007). doi:10.1016/j.matlet.2006.12.089
14. X. Pang, I. Zhitomirsky, Mater. Charact. **58**, 339 (2007). doi:10.1016/j.matchar.2006.05.011
15. S. Roessler, R. Born, D. Scharnweber, H. Worch, A. Sewing, M. Dard, J. Mater. Sci.: Mater. Med. **12**, 871 (2001). doi:10.1023/A:1012807621414
16. H. Schliephake, D. Scharnweber, M. Dard, S. Rossler, A. Sewing, C. Huttmann, J. Biomed. Mater. Res. **64**, 225 (2003). doi:10.1002/jbm.a.10363
17. H.B. Hu, C.J. Lin, R. Hu, Y. Leng, Mater. Sci. Eng. C **20**, 209 (2002). doi:10.1016/S0928-4931(02)00035-8
18. J. Redepenning, G. Venkataraman, J. Chen, N. Stafford, J. Biomed. Mater. Res. A **66**, 411 (2003). doi:10.1002/jbm.a.10571
19. J. Wang, J. De Boer, K. DeGroot, J. Dent. Res. **83**, 296 (2004)
20. X. Pang, I. Zhitomirsky, Int. J. Nanosci. **4**, 409 (2005). doi:10.1142/S0219581X05003176
21. X.F. Xiao, R.F. Liu, X.L. Tang, J. Mater. Sci.: Mater. Med. **19**, 175 (2008). doi:10.1007/s10856-007-0161-y
22. E.M. Carlisle, Science **167**, 179 (1970). doi:10.1126/science.167.3916.279

23. I.R. Gibson, S.M. Best, W. Bonfield, J. Biomed. Mater. Res. **44**, 422 (1999). doi :10.1002/(SICI)1097-4636(19990315)44:4<422::AID-JBM8>3.0.CO;2-#
24. N. Patel, S.M. Best, W. Bonfield, I.R. Gibson, K.A. Hing, E. Damien, P.A. Revell, J. Mater. Sci.: Mater. Med. **13**, 1199 (2002). doi:10.1023/A:1021114710076
25. S.R. Kim, J.H. Lee, Y.T. Kim, D.H. Riu, S.J. Jung, Y.J. Lee, S.C. Chung, Y.H. Kim, Biomaterials **24**, 1389 (2003). doi:10.1016/S0142-9612(02)00523-9
26. D. Arcos, J. Rodriguez-Carvajal, M. Vallet-Regi, Chem. Mater. **16**, 2300 (2004). doi:10.1021/cm035337p
27. E.S. Thian, J. Huang, S.M. Best, Z.H. Barber, W. Bonfield, Biomaterials **26**, 2947 (2005). doi:10.1016/j.biomaterials.2004.07.058
28. A.P.D. Elfick, Biomaterials **23**, 4463 (2002). doi:10.1016/S0142-9612(02)00163-1
29. H.W. Kim, Y. Deng, P. Miranda, A. Pajares, D.K. Kim, H.E. Kim, B.R. Lawn, J. Am. Ceram. Soc. **84**, 2377 (2001)
30. X.L. Tang, X.F. Xiao, R.F. Liu, Mater. Lett. **59**, 3841 (2005). doi:10.1016/j.matlet.2005.06.060
31. T. Kokubo, H. Takadama, Biomaterials **27**, 2907 (2006). doi:10.1016/j.biomaterials.2006.01.017
32. T. Kokubo, Biomaterials **2**, 155 (1991). doi:10.1016/0142-9612(91)90194-F